Hybrid nanoplasmonic-photonic resonators for efficient coupling of light to single plasmonic nanoresonators

Maysamreza Chamanzar* **and Ali Adibi**

School of Electrical and Computer Engineering, Georgia Institute of Technology, Atlanta, GA 30332, USA

*chamanzar@gatech.edu

Abstract: We show that efficient coupling of lightwave is possible to an individual plasmonic nanoresonator in a hybrid plasmonic-photonic resonator structure. The proposed hybrid structure consists of a photonic microresonator strongly coupled to a plasmonic nanoresonator. The theory and simulation results show that more than 73% of the input power in the waveguide can be coupled to the localized resonance mode of the plasmonic nanoresonator.

© 2011 Optical Society of America

OCIS codes: (230.5750) Resonators; (240.6680) Surface plasmons; (230.3120) Integrated optics devices.

References and links

1. N. Rosi and C. Mirkin, "Nanostructures in biodiagnostics," Chem. Rev. **105**, 1547–1562 (2005).
2. M. Juan, M. Righini, and R. Quidant, "Plasmon nano-optical tweezers," Nat. Photonics **5**, 349–356 (2011).
3. N. Lindquist, P. Nagpal, A. Lesuffleur, D. Norris, and S. Oh, "Three-dimensional plasmonic nanofocusing," Nano Lett. **10**, 1369–1373 (2010).
4. R. Tripp, R. Dluhy, and Y. Zhao, "Novel nanostructures for SERS biosensing," Nano Today **3**, 31–37 (2008).
5. H. Atwater and A. Polman, "Plasmonics for improved photovoltaic devices," Nat. Mater. **9**, 205–213 (2010).
6. W. Challener, C. Peng, A. Itagi, D. Karns, W. Peng, Y. Peng, X. Yang, X. Zhu, N. Gokemeijer, Y. Hsia, G. Ju, R. E. Rottmayer, M. A. Seigler, and E. C. Gage, "Heat-assisted magnetic recording by a near-field transducer with efficient optical energy transfer," Nat. Photonics **3**, 220–224 (2009).
7. S. Maier and H. Atwater, "Plasmonics: Localization and guiding of electromagnetic energy in metal/dielectric structures," J. Appl. Phys. **98**, 011101 (2005).
8. X. Huang, I. El-Sayed, W. Qian, and M. El-Sayed, "Cancer cell imaging and photothermal therapy in the near-infrared region by using gold nanorods," J. Am. Chem. Soc. **128**, 2115–2120 (2006).
9. K. Kelly, E. Coronado, L. Zhao, and G. Schatz, "The optical properties of metal nanoparticles: the influence of size, shape, and dielectric environment," J. Phys. Chem. B **107**, 668–677 (2003).
10. P. Stiles, J. Dieringer, N. Shah, and R. Van Duyne, "Surface-enhanced Raman spectroscopy," Annu. Rev. Anal. Chem. **1**, 601–626 (2008).
11. A. McFarland and R. Van Duyne, "Single silver nanoparticles as real-time optical sensors with zeptomole sensitivity," Nano Lett. **3**, 1057–1062 (2003).
12. G. Raschke, S. Kowarik, T. Franzl, C. Sonnichsen, T. Klar, J. Feldmann, A. Nichtl, and K. Kurzinger, "Biomolecular recognition based on single gold nanoparticle light scattering," Nano Lett. **3**, 935–938 (2003).
13. L. Sherry, R. Jin, C. Mirkin, G. Schatz, and R. Van Duyne, "Localized surface plasmon resonance spectroscopy of single silver triangular nanoprisms," Nano Lett. **6**, 2060–2065 (2006).
14. M. Chamanzar, M. Soltani, B. Momeni, S. Yegnanarayanan, and A. Adibi, "Hybrid photonic surface-plasmon-polariton ring resonators for sensing applications," Appl. Phys. B **101**, 263–271 (2010).
15. B. Min, E. Ostby, V. Sorger, E. Ulin-Avila, L. Yang, X. Zhang, and K. Vahala, "High-Q surface-plasmon-polariton whispering-gallery microcavity," Nature **457**, 455–458 (2009).
16. I. White, H. Oveys, and X. Fan, "Increasing the enhancement of SERS with dielectric microsphere resonators," Spectroscopy Mag. **21**, 1–5 (Apr. 2006).

#151465 - $15.00 USD Received 22 Jul 2011; revised 18 Oct 2011; accepted 18 Oct 2011; published 24 Oct 2011

17. S. Zou and G. C. Schatz, "Combining micron-size glass spheres with silver nanoparticles to produce extraordinary field enhancements for surface-enhanced Raman scattering applications," Israel J. Chem. **46**, 293–297 (2006).
18. F. De Angelis, M. Patrini, G. Das, I. Maksymov, M. Galli, L. Businaro, L. Andreani, and E. Di Fabrizio, "A Hybrid plasmonic-photonic nanodevice for label-free detection of a few molecules," Nano Lett. **8**, 2321–2327 (2008).
19. M. Barth, S. Schietinger, S. Fischer, J. Becker, N. Nusse, T. Aichele, B. Lochel, C. Sonnichsen, and O. Benson, "Nanoassembled plasmonic-photonic hybrid cavity for tailored light-matter coupling," Nano Lett. **10**, 891–895 (2010).
20. S. Boriskina and B. Reinhard, "Spectrally and spatially configurable superlenses for optoplasmonic nanocircuits," Proc. Natl. Acad. Sci. U.S.A. **108**, 3147–3151 (2011).
21. S. I. Shopova, R. Rajmangal, S. Holler, and S. Arnold, "Plasmonic enhancement of a whispering-gallery-mode biosensor for single nanoparticle detection," Appl. Phys. Lett. **98**, 243104 (2011).
22. M. A. Santiago-Cordoba, S. V. Boriskina, F. Vollmer, and M. C. Demirel, "Nanoparticle-based protein detection by optical shift of a resonant microcavity," Appl. Phys. Lett. **99**, 073701 (2011).
23. H.T. Hattori, Z. Li, D. Liu, I. D. Rukhlenko, and M. Premaratne, "Coupling of light from microdisk lasers into plasmonic nano-antennas," Opt. Express **17**, 20878–20884 (2009).
24. P. Yeh, *Optical Waves in Layered Media* (Wiley Online Library, 1988), Vol. 95.
25. Y. Xu, Y. Li, R. Lee, and A. Yariv, "Scattering-theory analysis of waveguide-resonator coupling," Phys. Rev. E **62**, 7389–7404 (2000).
26. K. Vahala, "Optical microcavities," Nature **424**, 839–846 (2003).
27. P. Deotare, M. McCutcheon, I. Frank, M. Khan, and M. Lončar, "High quality factor photonic crystal nanobeam cavities," Appl. Phys. Lett. **94**, 121106 (2009).

1. Introduction

Nanoplasmonic structures have been the subject of intensive recent research. They have been used in a variety of applications such as biochemical sensing [1], optical trapping and manipulation [2], nanofocusing [3], surface enhanced Raman spectroscopy (SERS) [4], energy harvesting [5], localized heating [6], nonlinear optics [7], and photothermal cancer therapy [8]. Plasmonic nanoresonators can localize the lightwave beyond the diffraction limit. The very localized surface plasmons in these structures result in ultra-high field enhancements. Localized surface plasmon resonance (LSPR) modes are excited as a result of resonant oscillation of free electrons on the surface of plasmonic nanoresonators coherent with the incident lightwave at certain resonance frequencies. The resonance properties of plasmonic nanoresonators depend on their size, shape, and the material properties [9]. Plasmonic nanoresonators are usually interrogated collectively either in a solution or when immobilized on a surface [10]. It has been shown that by using individual plasmonic nanoparticles, highly improved detection limits approaching the single molecule limit can be achieved [11, 12]. Also, the ability to excite and detect individual plasmonic nanoresonators makes the study of resonance properties of plasmonic nanoresonators possible without the interference of collective effects of the ensemble of nanoresonators. However, excitation of individual plasmonic nanoresonators using free-space optics is not efficient, and the signal-to-noise-ratio is very small. This renders extinction spectroscopy of individual plasmonic nanoresonators almost impossible [11]. It has been shown that a darkfield microscope can be used to interrogate individual plasmonic nanoresonators by using scattering spectroscopy [12, 13]. This still requires a very sensitive detector and a bulky microscope system with a precise alignment control. The inefficient coupling of the lightwave to each individual plasmonic nanoresonator reduces the signal-to-noise-ratio in sensing and spectroscopy applications; and it also limits the level of possible field enhancement, which is necessary for efficient light-matter interaction. Also, the bulky darkfield microscope systems and very sensitive detectors for scattering spectroscopy limit the scope of practical applications of plasmonic nanoresonators. To harness the advantages of plasmonic nanoresonators for practical applications, it is essential to improve the coupling of the lightwave to the localized surface plasmon resonance modes. Also, a robust, reliable, and alignment-insensitive method

#151465 - $15.00 USD Received 22 Jul 2011; revised 18 Oct 2011; accepted 18 Oct 2011; published 24 Oct 2011
(C) 2011 OSA

for the excitation and detection of individual plasmonic nanoresonators must be adopted.

In a previous work, We have shown that by using on-chip photonic integrated structures, whispering gallery surface plasmon polariton (SPP) resonance modes of metallic strip ring resonators can be efficiently excited [14]. It was shown that the photonic microresonator modes can provide the necessary momentum to excite the SPP modes. Bumki Min, et al. have also shown that by coating a silica microdisk with a layer of silver, whispering gallery SPPs can be supported at the interface of silica and silver, which can have high quality factors as high as $Q = 1800$ [15]. It has been shown that if a silica microsphere is immersed in a solution consisting of a mixture of silver nanoparticles and Rhodamine 6G (R6G) molecules, then the Raman emission of R6G molecules attached to silver nanoparticles can be enhanced [16]. This experiment has demonstrated that the whispering gallery modes of a microsphere can excite the near-field plasmonic resonance of the silver nanoparticles attached to the surface of the microsphere. In this experiment, silver nanoparticles attach to the surface of the microsphere randomly and form clusters. Also, extraordinary field enhancements have been shown possible by combining glass microspheres and silver nanoparticles for surface enhanced Raman sensing [17]. A plasmonic nanoantenna with an ogival-shape tip combined with a planar photonic crystal cavity has also been demonstrated [18]. The nanoantenna focuses the incident light into a nanoscale region to interact with the molecules and the photonic crystal cavity couples the intrinsically evanescent SPP mode of the nanoantenna to a propagating mode that can be detected as far-field scattering. This device is excited using out-of-plane incidence and can be used as a near-field probe. A nanoassembled plasmonic-photonic hybrid cavity has been demonstrated [19] that consists of a planar photonic crystal cavity and plasmonic nanostructures that are placed inside the cavity by using an AFM tip. It has been shown that the Purcell factor of this hybrid cavity is one order of magnitude larger than that of a bare photonic crystal cavity. The plasmonic nanoparticles can be accurately placed on top of the photonic crystal cavity. However, this method of hybridization cannot be easily used for making practical devices. In each of the last two examples, a planar photonic crystal cavity was used as the photonic structure that is excited using out-of-plane incidence. Although planar photonic crystal cavities have shown large Purcell factors, the lack of an efficient on-chip excitation mechanism has limited their application. Boriskina et al., have also recently demonstrated a reconfigurable optoplasmonic superlens based on photonic microspheres and plasmonic nanospheres for enhancing dipole radiative rates [20]. The sensitivity enhancement of a whispering-gallery-mode biosensor by using plasmonic nanoparticles is recently demonstrated [21, 22]. The possibility of coupling of light from a microdisk laser to a waveguide and then to a nanoantenna is also numerically studied [23].

In this paper, we discuss the theoretical design of a novel photonic-plasmonic hybrid resonator in which photonic whispering gallery modes are efficiently coupled to plasmonic nanoresonator LSPR modes. The proposed ultra-compact device can be implemented on a chip in an integrated platform. This structure is not alignment sensitive, and the excitation and detection does not require bulky free-space optics. We show that by optimization of the hybrid structure, coupling efficiencies as high as 73% can be achieved for coupling of light to a single plasmonic nanoresonator. The proposed hybrid structure can be used as an efficient functional lab-on-chip platform for biochemical sensing, energy harvesting, on-chip signal processing, and communications. In Section 2, we discuss the proposed hybrid plasmonic-photonic resonator structure, and the principle of operation. In Section 3, the theoretical model and the design procedure is presented. In Section 4, a discussion of the performance of the device, and its optimization will be given. Conclusions will be given in Section 5.

#151465 - $15.00 USD Received 22 Jul 2011; revised 18 Oct 2011; accepted 18 Oct 2011; published 24 Oct 2011
(C) 2011 OSA

2. Hybrid plasmonic-photonic resonator structure

The schematic of the proposed hybrid photonic-plasmonic structure is shown in Fig. 1. It consists of a photonic microresonator integrated with a plasmonic nanoresonator. The whispering gallery mode of the photonic microresonator is coupled to the LSPR mode of the plasmonic nanoresonator mode. The plasmonic nanoresonator can be of any shape, e.g., nanodisk, nanorod, bowtie antenna, dimer; and it can be made of any plasmonic material such as gold and silver. In this paper, we assume that the plasmonic nanoresonator is a gold nanorod. It can provide large field enhancements, and its resonance wavelength can be tuned over a large range by changing the aspect ratio of the nanorod. The plasmonic nanorod has dimensions of $(d_1 \times d_2 \times t)$, and the radius of curvature of the nanorod is assumed to be half of its width, i.e., $(\frac{d_2}{2})$. The same design concept applies to other plasmonic nanoresonators in this hybrid structure. The photonic microresonator is assumed to be a Si_3N_4 microring resonator with a cross section of $(w \times h)$ and an outer radius of R. Microrings can be easily designed to have a single radial mode at the operation wavelength of interest. Si_3N_4 has a relatively large refractive index, and also it is transparent in a wide range of frequencies ranging from visible to near-infrared, which makes it an appropriate material of choice for light-matter interaction and sensing. A ridge waveguide carries the lightwave on the chip and couples it to the hybrid plasmonic-photonic structure. The substrate is silicon dioxide (SiO_2). The polarization of interest is TE-like with an electric field parallel to the longer dimension of the nanorod.

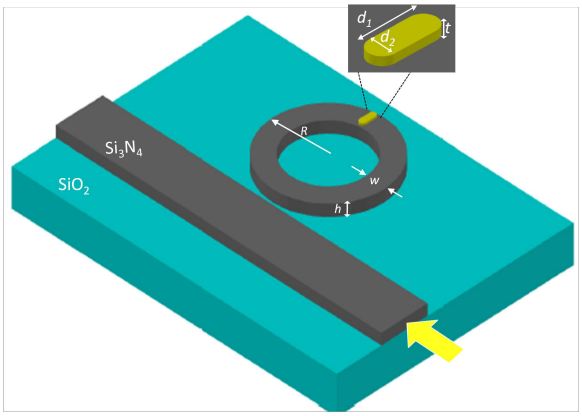

Fig. 1. Schematic of a hybrid plasmonic-photonic double-resonator structure consisting of a microresonator integrated with a plasmonic nanoresonator.

Photonic microresonators can have high quality factors (Qs), and therefore, narrow resonance lineshapes. However, the physical size and the mode volume of them are large. On the other hand, plasmonic nanoresonators having extremely small sizes can enhance the lightwave intensity by several orders of magnitude. However, the resonance features of these plasmonic nanoresonators are broadband. The very small size of the plasmonic nanoresonators makes the coupling of lightwave energy to the resonance modes of these nanoresonators difficult and inefficient. The hybrid structure introduced here is designed to benefit from the best of the two photonic and plasmonic resonators. In this double-resonator structure, lightwave is enhanced in two steps. It is first coupled to the high-Q microresonator, where it gets enhanced, and then it is efficiently coupled to the plasmonic nanoresonator.

In a practical situation, the input available power is limited, and it is important to couple this input power to the LSPR mode of the plasmonic nanoresonator structure efficiently. The highest field enhancement is achievable when the maximum possible power is coupled to the

#151465 - $15.00 USD Received 22 Jul 2011; revised 18 Oct 2011; accepted 18 Oct 2011; published 24 Oct 2011
(C) 2011 OSA

plasmonic nanoresonator LSPR mode. In cases where the plasmonic nanoresonators are excited using free-space optics, it is therefore important to tightly focus the lightwave to maximize the amount of light coupled to each individual plasmonic nanoresonator. It has been shown that by using a planar solid immersion mirror, light can be efficiently coupled to a plasmonic near-field transducer (NFT) for dense recording of magnetic memories [6]. It has been theoretically shown that about 8% coupling efficiency, defined as the fraction of the focused input power dissipated in the medium through the NFT, is possible [6]. Here, we define the coupling efficiency as the ratio of the power coupled to the plasmonic nanoresonator mode to the input power. We show that by properly designing the hybrid structure, we can achieve large coupling efficiencies.

3. Theoretical model and design

The design goal is to maximize the lightwave power that is coupled from the waveguide to the single plasmonic nanoresonator mode shown in Fig. 1. The schematic of the hybrid resonator structure with forward and backward propagating waves indicated at different points is shown Fig. 2. Forward and backward propagating waves at different points are related to each other through scattering matrices [24]. Existence of the plasmonic nanoresonator can result in the coupling of clockwise and counterclockwise modes in the photonic microresonator. Therefore, both modes are considered in the analysis.

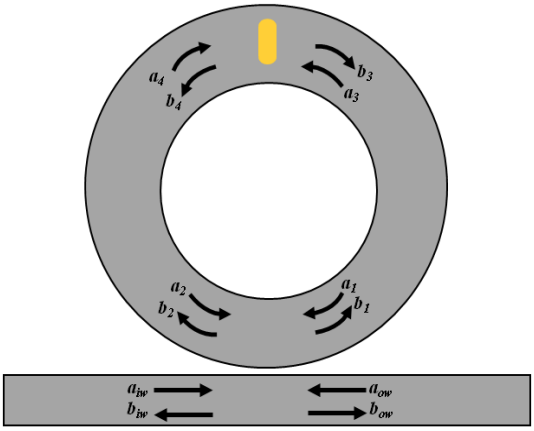

Fig. 2. Two-dimensional schematic of a hybrid plasmonic-photonic double-resonator structure consisting of a microring resonator integrated with a plasmonic nanoresonator. Forward and backward propagating field amplitudes are indicated at different points on the structure.

The incident lightwave in the waveguide (a_{iw}) is coupled to the counterclockwise whispering gallery mode of the photonic microresonator (b_1), which propagates around the microresonator, and becomes (a_3). Part of the lightwave incident on the nanororesonator is coupled to the plasmonic nanoresonator mode and the rest is either reflected (b_3), or transmitted (b_4). These lightwaves propagate in opposite directions around the microring resonator. Part of the counterclockwise mode is then coupled to the waveguide in the forward direction. Similarly, part of the clockwise mode is coupled to the waveguide in the backward direction, which forms the reflection. It should be noted that in steady state, all these lightwaves exist simultaneously. If there is no incident lightwave in the waveguide in the counter-propagating direction, then $a_{ow} = 0$. However, to keep the generality of the analysis, all the forward and the backward propagating waves available in the analysis are retained, and they will be made equal to zero whenever necessary in the numerical implementation. This is particularly useful when the waveguide itself

#151465 - $15.00 USD Received 22 Jul 2011; revised 18 Oct 2011; accepted 18 Oct 2011; published 24 Oct 2011
(C) 2011 OSA

is part of another microresonator.

The lightwaves in the waveguide can be related to the lightwaves in the microring resonator as

$$\begin{bmatrix} b_{ow} \\ b_1 \end{bmatrix} = \begin{bmatrix} t & j\kappa \\ j\kappa & t^* \end{bmatrix} \begin{bmatrix} a_{iw} \\ a_2 \end{bmatrix}, \tag{1}$$

and

$$\begin{bmatrix} b_{iw} \\ b_2 \end{bmatrix} = \begin{bmatrix} t & j\kappa \\ j\kappa & t^* \end{bmatrix} \begin{bmatrix} a_{ow} \\ a_1 \end{bmatrix}. \tag{2}$$

These coupling matrices are unitary, i.e. $|\kappa|^2 + |t|^2 = 1$. The coupling coefficient from waveguide to the hybrid resonator is related to the coupling Q (Q_c) through $\kappa^2 = \frac{4\pi^2 R n_g}{\lambda_0 Q_c}$, with n_g being the group index, and λ_0 being the resonance wavelength. The lightwaves near the plasmonic nanoresonator in the microresonator, a_3 and a_4, are related to the lightwaves b_1 and b_2, through the propagation matrix, $[P_1]$ as

$$\begin{bmatrix} a_3 \\ a_4 \end{bmatrix} = [P_1] \begin{bmatrix} b_1 \\ b_2 \end{bmatrix}, \tag{3}$$

where

$$[P_1] = \begin{bmatrix} \exp(-j\beta L_1 - \alpha L_1) & 0 \\ 0 & \exp(+j\beta L_2 - \alpha L_2) \end{bmatrix}. \tag{4}$$

In Eq. (4), the propagation constant in the microresonator is indicated by β, and the loss decay constant by α. The loss decay constant is related to the intrinsic quality factor of the photonic microresonator, Q_0, through $\alpha = \frac{\pi n_g}{Q_0 \lambda_0}$. The average length of the microresonator from the waveguide-microresonator coupling point to the plasmonic nanoresonator location is indicated by L_1, and the average length of the microresonator from the plasmonic nanoresonator location to the waveguide-microresonator coupling point is indicated by L_2.

Similarly, the lightwaves, a_1 and a_2 are related to the lightwaves b_3 and b_4, through the propagation matrix, $[P_2]$ as

$$\begin{bmatrix} a_1 \\ a_2 \end{bmatrix} = [P_2] \begin{bmatrix} b_3 \\ b_4 \end{bmatrix}, \tag{5}$$

where $[P_2]$ is the propagation matrix accounting for the phase shift and loss of the lightwaves propagating from the nanoresonator to the waveguide-microresonator coupling point. The lightwaves in the microresonator next to the plasmonic nanoresonator are related to each other as

$$\begin{bmatrix} a_4 \\ b_4 \end{bmatrix} = [M] \begin{bmatrix} a_3 \\ b_3 \end{bmatrix}, \tag{6}$$

where $[M]$ is a matrix that accounts for the coupling of the clockwise and counterclockwise propagating lightwaves to the LSPR mode of the plasmonic nanoresonator, as well as the reflection and the transmission from the nanoresonator. The portion of the hybrid resonator that consists of the plasmonic nanorod coupled to the microresonator can be locally assumed to be a hybrid waveguide, consisting of a plasmonic nanoresonator coupled with a ridge waveguide, and it can be modeled as a standing wave resonator to obtain $[M]$ [25]. The only difference is that here, the waveguide is excited using counter-propagating waves from both sides. According to Fig. 3, matrix $[M]$ can be constructed as

#151465 - $15.00 USD Received 22 Jul 2011; revised 18 Oct 2011; accepted 18 Oct 2011; published 24 Oct 2011
(C) 2011 OSA

$$[M] = \begin{bmatrix} \frac{-jr_p}{t_p} & \frac{1}{t_p} \\ \frac{t_p^2+r_p^2}{t_p} & \frac{-jr_p}{t_p} \end{bmatrix}, \tag{7}$$

where r_p and t_p are the reflection and the transmission coefficients for the hybrid waveguide structure when excited from each side.

Fig. 3. The portion of the hybrid structure in Fig. 2 consisting of the plasmonic nanoresonator is modeled as a hybrid waveguide-based structure, which is excited from both ends.

Finite difference time domain analysis (FDTD) can be used here to accurately obtain the reflection and the transmission coefficients, r_p and t_p. In addition, different lightwave fields can be obtained at different points throughout the hybrid resonator structure. For example, the field amplitude (b_1) in the photonic microresonator can be obtained as

$$\frac{b_1}{a_{iw}} = j\kappa \frac{1 - tt_p \exp(-\alpha L)\exp(\beta L)}{1 - tt_p \exp(-\alpha L)[\exp(\beta L) + \exp(-\beta L)] + t^2(r_p^2 + t_p^2)}, \tag{8}$$

The coupling efficiency, as mentioned in Section 2, is defined as the ratio of the power coupled to the plasmonic nanoresonator to the input power in the waveguide, and it can be expressed as

$$|k|^2 = \frac{(|a_3|^2 + |a_4|^2) - (|b_3|^2 + |b_4|^2)}{|a_{iw}|^2}. \tag{9}$$

In the hybrid resonator structure introduced in Fig. 1, the input lightwave is coupled to the plasmonic nanoresonator mode in two steps. In the first step, the lightwave is coupled to the photonic microresonator from the waveguide. In the second step, the lightwave is coupled from the microresonator to the LSPR mode of the nanoresonator. In order to design and analyze the hybrid structure, it is first assumed that the gap between the bus waveguide and the hybrid resonator is so large that the coupling between the two structures is weak, and the loading effect of the waveguide on the hybrid resonator structure can be neglected. The reflection and the transmission of the bus waveguide, for a hybrid resonator structure consisting of a $20\mu m$ radius microring with dimensions of ($w = 700nm$ and $h = 200nm$) integrated with a gold nanorod of dimensions ($100nm \times 56nm \times 30nm$), are plotted in Figs. 4(a) and 4(b), respectively for the two cases of photonic microresonator with and without the gold nanorod at the LSPR peak wavelength.

In these simulations, as a typical example, the intrinsic Q of the microresonator is assumed to be $Q_0 = 1.5 \times 10^4$. The Q_0 of the microring resonator is determined by the radiation loss, material absorption, and scattering loss from sidewalls and the top surface, determined by the quality of fabrication. The coupling Q to the waveguide depends on the distance between the waveguide and the microresonator, as well as the dimensions of the waveguide. The coupling Q is assumed to be $Q_c = 10^7$ here, which ensures the weak coupling between the waveguide and the microresonator structure. We will show that Q_c can be optimized for any given Q_0 to achieve high coupling efficiencies. It can be seen from Fig. 4(a) that the gold nanorod causes some part of the counterclockwise mode to be coupled to the clockwise mode in the microresonator, which

#151465 - $15.00 USD Received 22 Jul 2011; revised 18 Oct 2011; accepted 18 Oct 2011; published 24 Oct 2011
(C) 2011 OSA

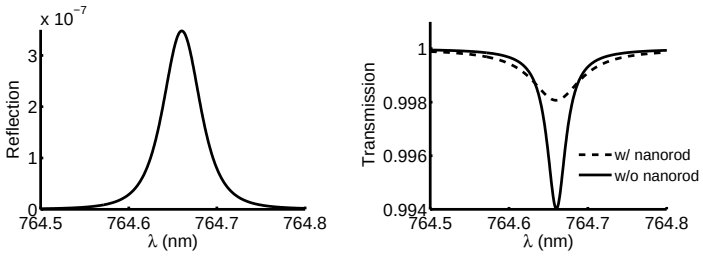

(a) (b)

Fig. 4. (a) Reflection and (b) transmission of a bus waveguide coupled to a hybrid resonator in weak coupling regime with $Q_c = 10^7$. The results are plotted for two cases, one with a nanorod and the other without a nanorod. No reflection occurs when there is no nanorod integrated with the microresonator.

is consequently coupled to the reflected lightwave. From the transmission spectrum, Fig. 4(b), it can be seen that the effect of the plasmonic nanorod is to broaden the resonance and lower the extinction.

It should be noted that in Eq. (8), r_p and t_p are functions of frequency and have resonance behaviors similar to the one shown in Fig. 5(a). Therefore, the lightwave amplitudes and consequently, the coupling efficiency defined in Eq. (9) are intricate functions of frequency. To better understand the frequency-dependent behavior of r_p and t_p, the plasmonic resonance spectrum of the gold nanorod ($100nm \times 56nm \times 30nm$) integrated with a waveguide of the same cross-sectional dimensions as those of the microring resonator, i.e., ($700nm \times 200nm$), is plotted in Fig. 5(a). This resonance lineshape is obtained from a 3D FDTD analysis of the equivalent hybrid waveguide structure. It can be seen that the LSPR wavelength is $\lambda = 764.5nm$, and the lineshape is broadband with a full width at half maximum (FWHM) of $91nm$.

To get more insight about the modes of the hybrid resonator structure, we study the response of the hybrid resonator structure both at an input wavelength close to the LSPR peak wavelength, point *A* in Fig. 5(a), and also at a wavelength far from the LSPR peak wavelength, point *B* in Fig. 5(a). Fig. 5(b) shows the coupling efficiency at the LSPR peak wavelength, point *A*, and Fig. 5(c) shows the coupling efficiency far from the LSPR peak wavelength at $\lambda = 845.7nm$, point *B*. It can be seen that far from the resonance of the plasmonic nanoresonator, the coupling efficiency exhibits a doublet response resulting from the coupling and splitting of the counter-propagating modes in the microresonator. As the incident wavelength deviates from the plasmonic nanoresonator LSPR peak wavelength, the splitting becomes stronger and the coupling efficiency decreases. Therefore, the splitting quality factor, $Q_s = \frac{\omega n_g 2\pi R}{|r_p|^2 c}$, can be used as a measure of the coupling efficiency. Here, ω is the angular frequency, n_g is the group index, R is the radius of the microring resonator, and c is the speed of light in free space. In both cases shown in Fig. 5(b) and Fig. 5(c), the clockwise and the counter-clockwise modes exist in the microresonator, and part of the input power is reflected back through the bus waveguide.

So far, the hybrid resonator is studied almost independently of the loading effect of the bus waveguide by assuming a large Q_c between the bus waveguide and the hybrid resonator. It can be seen from Fig. 5(b) that when the gap between the bus waveguide and the hybrid resonator is large, i.e., $Q_c = 10^7$, even at the LSPR peak resonance wavelength, only about 0.1% of the input power is coupled to the plasmonic nanoresonator mode.

To optimize the coupling between the bus waveguide and the hybrid resonator structure, the coupling efficiency to the plasmonic nanorod, $|k|^2$, is plotted in Fig. 6 versus Q_c between the waveguide and the hybrid resonator for a hybrid structure with the same parameters as those

#151465 - $15.00 USD Received 22 Jul 2011; revised 18 Oct 2011; accepted 18 Oct 2011; published 24 Oct 2011
(C) 2011 OSA

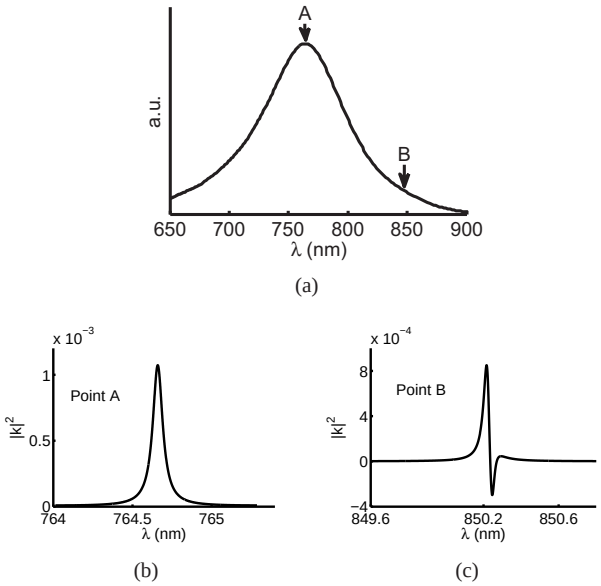

Fig. 5. (a) Plasmonic resonance lineshape of the gold nanorod ($100nm \times 56nm \times 30nm$) integrated with a waveguide of the same dimensions ($700nm \times 200nm$) as those of the microring resonator cross section. Coupling efficiency for a hybrid resonator with the same parameters as those used in Fig. 4, in the weak coupling regime, (a) near the LSPR resonance peak and (b) far from the LSPR resonance peak.

used in Fig. 5(a).

It can be seen that the coupling efficiency is maximized at a coupling Q of $Q_c = 6.7 \times 10^3$. The maximum coupling efficiency is more than 50%. To get a better insight into the coupling mechanism between the microring resonator and the plasmonic nanoresonator, the coupling efficiency spectrum, under the optimum conditions, i.e., $Q_c = 6.7 \times 10^3$ is plotted in Fig. 7(a), as the coupling efficiency , $|k|^2$, versus wavelength.

It can be seen that the envelope of the coupling efficiency spectrum follows the broadband resonance feature of the plasmonic nanoresonator LSPR mode on an equivalent waveguide. As shown in the inset of Fig. 7(b), this broadband envelope is sampled by the sharp resonances of the photonic microresonator. Using the proposed hybrid resonator structure, more than 50% coupling efficiency is possible to the plasmonic gold nanorod over several modes of the hybrid resonator structure that are separated by the free spectral range (FSR). The FSR = $1.2nm$ corresponds to the fundamental radial order modes of the microring resonator.

The presented analysis method, which is formulated in a matrix form, can be easily extended to the case where we have multiple plasmonic nanoresonators integrated with the photonic microresonator.

4. Discussion

So far, we have shown that by optimizing the hybrid resonator structure, the coupling efficiency can be optimized to a value of more than 50%, by assuming $Q_0 = 1.5 \times 10^4$. The coupling efficiency to the resonance mode of the plasmonic nanoresonator structure depends on the coupling quality factor between the waveguide and the hybrid resonator, Q_c, the intrinsic quality factor of the photonic microring resonator, Q_0, as well as the coupling between the photonic microres-

#151465 - $15.00 USD Received 22 Jul 2011; revised 18 Oct 2011; accepted 18 Oct 2011; published 24 Oct 2011
(C) 2011 OSA

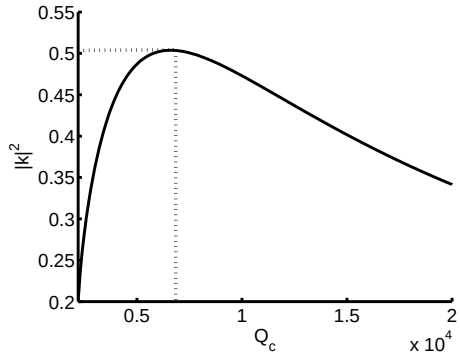

Fig. 6. Coupling efficiency for the hybrid resonator structure discussed in Fig. 5, versus the coupling quality factor, Q_c, between the waveguide and the hybrid resonator structure. The coupling efficiency is maximized at $Q_c = 6.7 \times 10^3$.

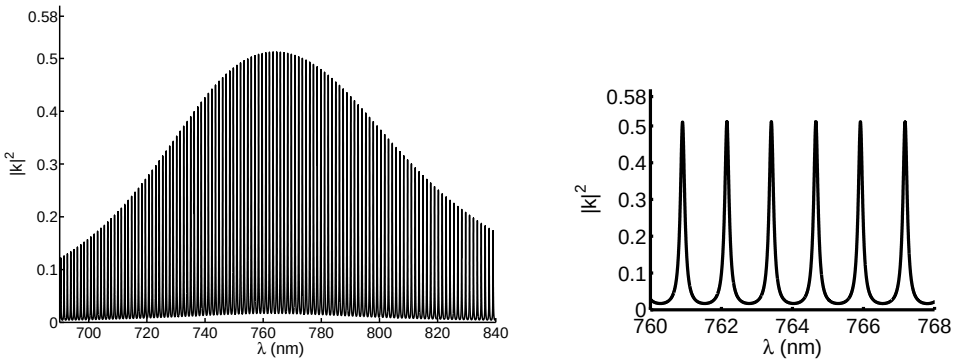

(a) (b)

Fig. 7. (a) Coupling efficiency spectrum over a large range of wavelengths under optimized conditions for the hybrid resonator structure discussed in Fig. 6 (i.e., $Q_c = 6.7 \times 10^3$). (b) The enlarged portion of the coupling efficiency spectrum near the plasmonic resonance peak, where several different modes of the hybrid structure can be seen having large coupling efficiencies.

onator and the plasmonic nanoresonator. It was shown in the previous section that the coupling between the waveguide and the hybrid resonator structure can be optimized to maximize the coupling efficiency to the plasmonic nanoresonator for a specific Q_0 of the photonic microresonator. In an ideal scenario, when the photonic microresonator is perfectly lossless, i.e., $Q_0 = \infty$, the coupling efficiency to the plasmonic nanoresonator can be obtained as

$$|k|^2 = |\kappa|^2 \frac{1-(t_p^2+r_p^2)}{|1-2tt_p+t^2(t_p^2+r_p^2)|^2}, \tag{10}$$

It can be seen that when the plasmonic nanoresonator is lossless, i.e., $t_p^2 + r_p^2 = 1$, the coupling efficiency is zero. In this case, there is no scattering or absorption of light by the nanoparticle; no power is removed from the lightwave circulating around the photonic microresonator; and the plasmonic nanoresonator would only cause the coupling of the clockwise and the counter-

#151465 - $15.00 USD Received 22 Jul 2011; revised 18 Oct 2011; accepted 18 Oct 2011; published 24 Oct 2011
(C) 2011 OSA

clockwise modes of the photonic microresonator. In practical situations, the scattering and the absorption cross section of plasmonic nanoresonators are nonzero, and the coupling efficiency indicates the ratio of the input power in the waveguide, which is coupled to the localized resonance mode of the plasmonic nanoresonator. Usually, $r_p \ll t_p$, since the extinction cross section of the plasmonic nanoresonators is very small. From Eq. (10), when $r_p \to 0$, the coupling efficiency approaches 100% asymptotically for an optimum value of $t = t_p$, or alternatively, $Q_c = \frac{4\pi^2 R n_g}{\lambda_0(1-t_p^2)}$. Here, we can see the advantage of using the photonic microresonator, where a reasonable Q_c results in efficient coupling of the input lightwave to a very low-Q plasmonic nanoresonator. Therefore, in an ideal situation, when the photonic microresonator is lossless, it is possible to couple almost all of the input light power to the localized surface plasmon resonance of the plasmonic nanoresonator mode. The only limitation would be the reflected power that is coupled back to the input waveguide through the clockwise propagating mode of the resonator. In practice, however, the photonic microresonator is not lossless and has a limited intrinsic quality factor, Q_0. To study the effect of the photonic microresonator intrinsic quality factor on the coupling of the lightwave to the plasmonic nanoresonator mode, the coupling efficiency is plotted versus the Q_0 and the Q_c in Fig. 8 at the resonance peak wavelength of $\lambda_0 = 764.65nm$.

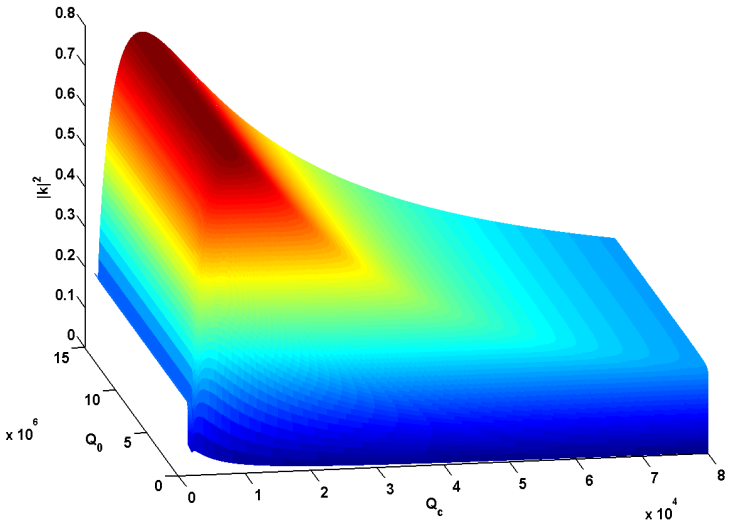

Fig. 8. Coupling efficiency as a function of the intrinsic quality factor (Q_0) and the coupling quality factor (Q_c) at the resonance peak wavelength of $\lambda_0 = 764.65nm$. It can be seen that the coupling efficiency has a maximum at each Q_0 for a specific value of Q_c.

It can be seen from Fig. 8 that the coupling efficiency has a maximum for each value of Q_0 at a specific Q_c from the waveguide, where the coupling of the lightwave from the bus waveguide to the hybrid resonator system and consequently from the photonic resonator to the plasmonic nanoresonator is maximized. It can also be observed that when Q_0 is increased, the coupling efficiency is increased. For example, at $Q_0 = 1.5 \times 10^7$ and $Q_c = 8.6 \times 10^3$ the coupling efficiency can reach a value of more than 77%. Even at these very high Q_0 values, where the loss of energy in the photonic microresonator is negligible, part of the lightwave is coupled to the clockwise travelling mode of the photonic microring resonator, and is subsequently coupled

#151465 - $15.00 USD Received 22 Jul 2011; revised 18 Oct 2011; accepted 18 Oct 2011; published 24 Oct 2011
(C) 2011 OSA

back to the bus waveguide as reflection. Achieving such high intrinsic quality factors is not easily possible in practice with the current quality of materials and fabrication processes. To investigate how practical is the proposed hybrid structure in efficiently coupling the lightwave to the plasmonic nanoresonator mode, the optimization surface, presented in Fig. 8, is plotted in the form of iso-$|k|^2$ contours in Fig. 9. It can be seen for example that at a $Q_0 = 1.37 \times 10^5$ and $Q_c = 8.6 \times 10^3$, the coupling efficiency is 73%, which still is large. The intrinsic quality factor of $Q_0 = 1.37 \times 10^5$ and the coupling quality factor of $Q_c = 8.6 \times 10^3$ are practically achievable. The proposed hybrid structure can also be extended to other photonic microresonator structures such as microdisk resonators, which have high quality factors. However, microdisk resonators usually have multiple radial modes, which makes the design more difficult. Other photonic microresonators such as microtoroids, microspheres, standing wave resonators, and photonic crystal cavities [26, 27] can also be used in the proposed architecture.

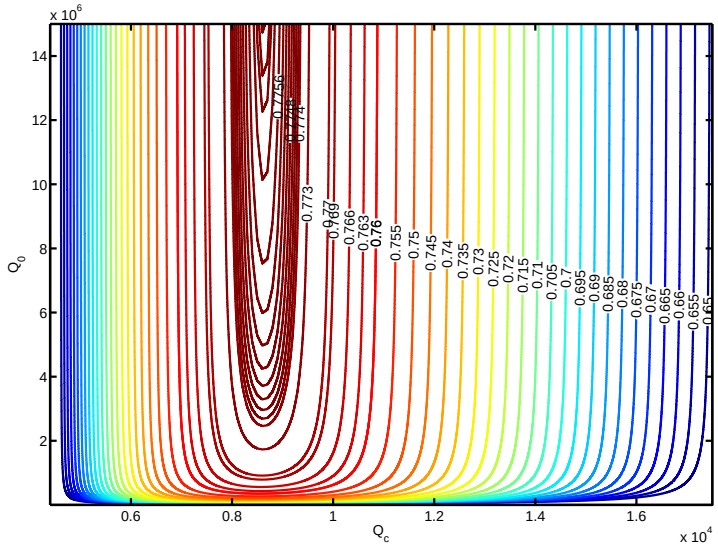

Fig. 9. Coupling efficiency as a function of the intrinsic quality factor, Q_0, and the coupling quality factor, Q_c at the resonance peak wavelength of $\lambda_0 = 764.65nm$. It can be seen that the coupling efficiency has a maximum at each intrinsic quality factor, Q_0, for a specific coupling quality factor, Q_c.

It should be noted that the total energy that is coupled to the resonance mode of the plasmonic nanoresonator and results in large near-field enhancements is partly absorbed by the metallic nanoresonator, and is partly scattered. Depending on the application of interest, the plasmonic nanoresonator can be designed to have either a large absorption cross section or a large scattering cross section. When a material is interacting with the enhanced near-field of the plasmonic nanoresonator, the energy can also be absorbed by the material. Here, we have demonstrated the results for a gold nanorod. The plasmonic nanoresonator shape, size, and material can be used to design different plasmonic nanoresonators with different absorption and scattering properties. It should also be noted that we have optimized the coupling of the lightwave to the dipole resonance mode of the plasmonic nanoresonator. The coupling efficiency can be optimized to higher order resonance modes, as well.

The large coupling efficiency to a single plasmonic nanoresonator mode greatly improves the field enhancement and signal-to-noise-ratio. This makes it possible to do practical individual

#151465 - $15.00 USD Received 22 Jul 2011; revised 18 Oct 2011; accepted 18 Oct 2011; published 24 Oct 2011
(C) 2011 OSA

plasmonic nanoresonator sensing by using low input powers. Also, the proposed hybrid structure can be realized on a chip, and is not alignment sensitive. Once the structure is implemented, excitation of the bus waveguide guarantees the excitation of the LSPR mode of the plasmonic nanoresonator. Also, the enhanced extinction of the hybrid resonator modes can be measured at the output of the bus waveguide. This eliminates the need for a bulky microscope with precise alignment control and a very sensitive detector to interrogate single plasmonic nanoresonators.

In the proposed hybrid resonator structure, the photonic microresonator with a large intrinsic quality factor, Q_0, facilitates the coupling of the lightwave from the bus waveguide to the plasmonic nanoresonator. In analogy to microwave antennas, the high-Q photonic microresonator can be considered as an impedance matching circuitry that optimizes the coupling of the input power to the plasmonic nanoresonator, which can be considered as a nanoantenna.

5. Conclusion

We have proposed, designed, and optimized a hybrid plasmonic-photonic resonator structure consisting of a plasmonic nanoresonator and a photonic microresonator, which can be used to efficiently couple the lightwave to the LSPR mode of the plasmonic nanoresonator. We have shown that by using the proposed hybrid structure, the coupling efficiency can be optimized so that more than 73% of the lightwave is coupled to a single gold nanorod. This greatly improves the signal-to-noise-ratio and the field enhancements. The improved signal-to-noise ratio is critically important for interrogation of single plasmonic nanoresonators in applications such as ultrasensitive sensing and spectroscopy. The on-chip and alignment-insensitive nature of the proposed structure makes it suitable for lab-on-chip applications, where a portable, low power, and compact device is desired. Also, since the broadband resonance signature of the plasmonic nanoresonator is enhanced by the photonic microresonator resonance modes, the extinction can be easily measured from the transmission spectrum. Therefore, to study the resonance behavior of single plasmonic nanoresonators, the transmission spectrum of the bus waveguide can be used, alleviating the need for locating and measuring the scattering of the single nanoresonator. The proposed device is compact, and the hybrid resonator can be implemented in a $40\mu m \times 40\mu m$ footprint. Therefore, many of them can be integrated on the same chip for multianalyte sensing. Also, the proposed hybrid plasmonic-photonic structure can employ the potentials of nanoplasmonic structures efficiently to bridge the gap between the nano-scale world of electronics and the larger-scale world of photonics. Therefore, we believe that our proposed hybrid platform can be used in different on-chip applications such as lab-on-chip sensing systems, on-chip spectroscopy, signal processing, and communications.

Acknowledgments

This work was supported by the Defense Advanced Research Projects Agency (DARPA) under Contract HR 0011-10-1-0075 through the DARPA CIPHER Project (S. Rodgers). The authors would like to thank Qing Li for helpful discussions.

#151465 - $15.00 USD Received 22 Jul 2011; revised 18 Oct 2011; accepted 18 Oct 2011; published 24 Oct 2011
(C) 2011 OSA